VIP Porous Frameworks

DOI: 10.1002/ange.201103493

Supercapacitive Energy Storage and Electric Power Supply Using an Aza-Fused π-Conjugated Microporous Framework**

*Yan Kou, Yanhong Xu, Zhaoqi Guo, and Donglin Jiang**

Supercapacitors are energy-storage and power-supply devices that are developed to meet the increasing demand for applications in powering vehicles and portable electronic devices.[1a] Supercapacitive energy storage operates on electric double layers by accumulation of charges at the electrode/electrolyte interfaces, at which the stored energy is proportional to the capacitance of the electrodes.[1b] Therefore, a breakthrough in electrode materials holds promise for fundamental advances in supercapacitor materials. As electrode materials, activated carbon has been intensively studied with capacitances up to 270 $F g^{-1}$.[2a] Recently, nanostructured carbon materials such as templated carbon materials, graphenes, carbon nanotubes, aerogels, and heteroatom-hybridized carbon materials have been developed with the aim to improve the performance and exhibit capacitances of 50–370 $F g^{-1}$.[2] Despite the extensive efforts in synthesis, the rational design of supercapacitive electrodes that meet large capacitance, high energy density, and outstanding stability remains a substantial challenge.

π-Conjugated microporous polymers (CMPs) are a class of porous frameworks consisting of an extended π-conjugated system and inherent nanopores.[3–7] As high surface-area porous materials, CMPs emerge as a new medium for gas adsorption and have been developed as a new type of nanoreactors and heterogeneous catalysts upon the integration of catalytic sites into the skeletons.[3–7] The extended π-conjugated system endows CMPs with noteworthy light-emitting properties and allows the construction of light-harvesting antennae that trigger efficient, rapid, and vectorial energy funneling from the skeleton to entrapped acceptors.[6b] From a synthetic point of view, CMPs are unique because they allow the elaborate control of both skeletons and pores. In this context, a promising way to the exploration of CMPs is to combine the structural advantages of a π-conjugated system and inherent pores. Herein, we report the synthesis of such co-operative porous frameworks based on aza-fused CMPs (Scheme 1, Aza-CMPs) and highlight their functions in supercapacitive energy storage and electric power supply.

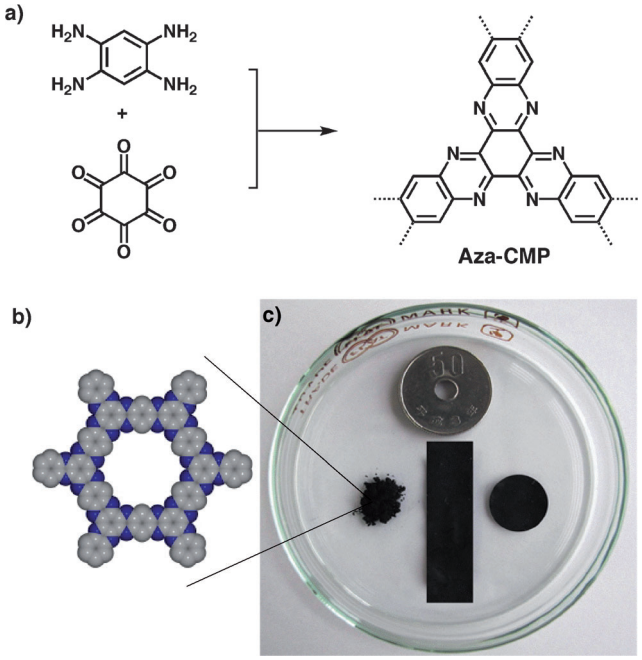

Scheme 1. a) Synthesis of an aza-fused π-conjugated microporous polymer (Aza-CMP). b) The elementary pore structure of Aza-CMPs calculated using the Gaussian 03 program at B3LYP/3-21G(d) level (the carbon network is gray and nitrogen is blue). c) Photographic image of the powder and flexible thin films with different shapes of Aza-CMPs.

Aza-CMPs comprise four features: 1) fused CMP frameworks that are conductive, 2) aza units in the skeletons that enable dipolar interaction with electrolyte cations[8] and accumulate protons on the walls of pores, 3) inherent micropores with optimized size that allows quick ion motion during charge–discharge processes, and 4) high surface areas provide large interfaces for the formation of electrostatic charge-separation layers in the pores. Ultimately, these structural features work co-operatively, leading to exceptional energy storage and power supply capacities.

Aza-CMPs were ionothermally synthesized by a condensation reaction of 1,2,4,5-benzenetetramine with triquinoyl hydrate at 300, 350, 400, 450, and 500 °C to give Aza-CMP@300, Aza-CMP@350, Aza-CMP@400, Aza-CMP@450, and Aza-CMP@500, respectively (Scheme 1, Aza-CMPs).

[*] Dr. Y. Kou, Y. Xu, Dr. Z. Guo, Prof. Dr. D. Jiang
Department of Materials Molecular Science
Institute for Molecular Science
National Institutes of Natural Sciences
5-1 Higashiyama, Myodaiji, Okazaki 444-8787 (Japan)
E-mail: jiang@ims.ac.jp
Prof. Dr. D. Jiang
Precursory Research for Embryonic Science and Technology (PRESTO)
Japan Science and Technology Agency (JST)
Chiyoda-ku, Tokyo 102-0075 (Japan)

[**] This work was supported by the Japan Science and Technology Agency (JST). D.J. acknowledges financial support from the Precursory Research for Embryonic Science and Technology (PRESTO) program of the JST.

Supporting information for this article is available on the WWW under http://dx.doi.org/10.1002/anie.201103493.

Infrared spectroscopy of Aza-CMPs indicated the presence of aza linkages in the network, whereas the vibration bands assigned to the amino and quinoyl groups of the monomers disappeared (see Figures S1 and S2 and Table S1 in the Supporting Information). Aza-CMPs consist of three types of carbon atoms, which are experimentally identified by ^{13}C cross-polarization/magic angle spinning NMR spectroscopy (see Figure S3 in the Supporting Information). Further characterization with X-ray photoelectron spectroscopy (XPS) also supported the structure. As exemplified by Aza-CMP@350, C 1s XPS revealed strong peaks at 285.9 and 287.9 eV, assigned to C=C and C=N units,[9] respectively (see Figures S4–S8 and Table S2 in the Supporting Information). In the N 1s XPS profiles, Aza-CMPs displayed a peak at 399.6 eV, which is close to that of hexaazatriphenylene (HAT, 399.9 eV, see Figure S9 in the Supporting Information).

Field-emission scanning electron microscopy (FE-SEM) revealed monolithic morphologies of sizes ranging from hundreds of nanometers to micrometers (Figure 1a and Figure S10 in the Supporting Information). Close observations of FE-SEM images at high magnification showed that the objects are basically comprised of monoliths. High-resolution transmission electron microscopy (HR-TEM) revealed that the monoliths consisted of a porous network structure (Figure 1b and Figure S11 in the Supporting Information). Enlargement of the HR-TEM image indicates pores with diameters less than 2 nm (Figure 1b, inset). In situ evaluation of the carbon and nitrogen distribution by elemental mapping with TEM revealed that both carbon (green) and nitrogen (violet) atoms exist homogeneously in the skeletons (Figure 1c–e and Figure S12 in the Supporting Information).

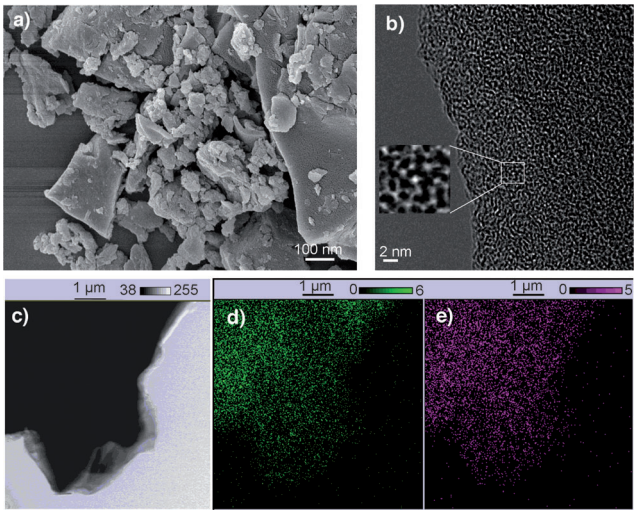

Figure 1. a) FE-SEM image of Aza-CMP@350. b) HR-TEM images of Aza-CMP@350. The inset shows an enlarged view of the pores. c) TEM image of Aza-CMP@350. d) Carbon atom mapping of the Aza-CMP@350 sample. e) Nitrogen atom mapping of the Aza-CMP@350 sample.

The pore structure was evaluated by nitrogen sorption isotherms measured at 77 K, which revealed that Aza-CMPs were microporous and exhibited typical type I reversible sorption profiles (Figure 2a). The pore parameters were dependent on the synthesis temperature T (Figure 2 and Table S3 in the Supporting Information). The BET (Brunauer–Emmett–Teller) specific surface area of Aza-CMP@300 was only 24 $m^2 g^{-1}$ (Figure 2c). The pore size as estimated by the Saito–Foley (SF) model[10] was 1.65 nm. In contrast, Aza-CMP@350 displayed an increased surface area of 546 $m^2 g^{-1}$ (Figure 2c), whereas the pore size was 1.4 nm (Figure 2b). The change was much more explicit for Aza-CMP@400, of which the BET surface area was as high as 1029 $m^2 g^{-1}$ and the pore size was decreased to 0.9 nm (Figure 2c). Synthesis at temperatures over 400 °C resulted in gradual leveling of the specific surface area to 1227 $m^2 g^{-1}$ as observed for Aza-CMP@500 (Figure 2c).

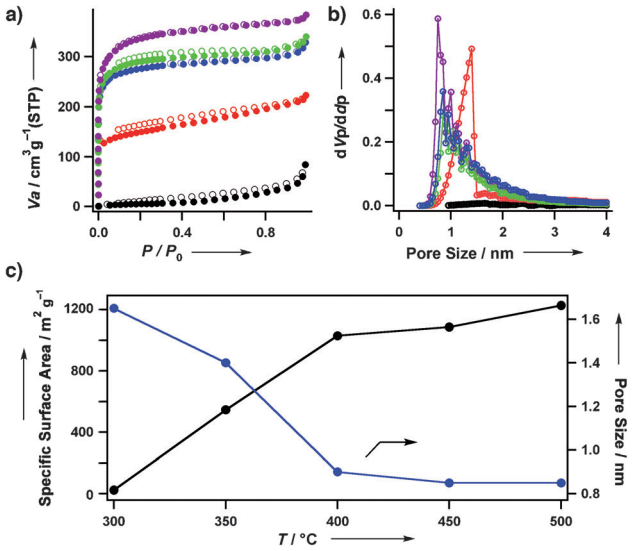

Figure 2. a) Nitrogen sorption curves (filled circles: adsorption, open circles: desorption, STP = standard temperature pressure) and b) pore size of Aza-CMP@300 (black), Aza-CMP@350 (red), Aza-CMP@400 (blue), Aza-CMP@450 (green), and Aza-CMP@500 (purple). c) Plot of the BET surface area and pore size versus synthesis temperature.

Aza-CMPs are amorphous and do not show clear peaks in X-ray powder diffraction measurements (see Figure S13 in the Supporting Information). Free-standing flexible thin films (Scheme 1c) of Aza-CMPs were easily prepared using the traditional electrode preparation method (Supporting Information). These film electrodes can easily be cut to different shapes and sizes (Scheme 1c). Disk-shaped films were used as the working electrodes for electrochemical measurements in a standard 1 M H_2SO_4 solution as aqueous electrolyte (Supporting Information). Cyclic voltammetry (CV) measurements of the HAT films gave a horizontal I–V curve. This curve did not exhibit a change in current with voltage (Figure 3a, black curve), which indicates that HAT is inactive for capacitive energy storage. In sharp contrast, Aza-CMP@350 exhibited symmetric I–V curves and afforded reversible voltage-dependent current loops, typical of the supercapacitive energy storage (Figure 3a). These results suggest that the CMP structure is essential for energy storage. One significant feature of the I–V profiles (Figure 3a) is that no redox peaks

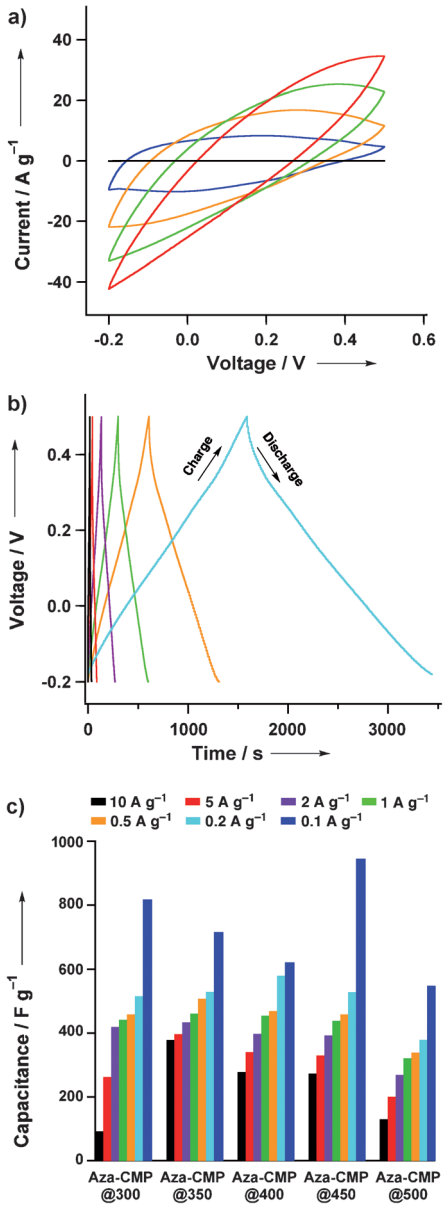

Figure 3. a) Cyclic voltammetric profiles of Aza-CMP@350 at scan rates of 25 (blue), 50 (orange), 100 (green), and 200 mV s^{-1} (red), and hexaazatriphenylene (HAT) at a scan rate of 100 mV s^{-1} (black). b) Charge–discharge profiles of Aza-CMP@350 at current densities of 10 (black), 5 (red), 2 (purple), 1 (green), 0.5 (orange), and 0.2 A g^{-1} (blue), respectively. c) Capacitance of Aza-CMPs at different current densities.

are observable, which indicates that Aza-CMPs do not involve redox-related faradic processes during the charge–discharge process. The *I*–*V* curves of Aza-CMP@350 at the different scan speeds retain good symmetry, which confirms good electrochemical stability and capacitance.[11] Other Aza-CMPs also show an increased current with increased scan speed (see Figure S14 in the Supporting Information).

The supercapacitive performance was tested with galvanostatic charge–discharge cycling experiments. Figure 3b shows typical charge–discharge profiles for Aza-CMP@350. For example, the profile recorded at a current density of 0.2 A g^{-1} (blue curve) shows a linear increase in voltage with time during the charge process and again a linear decrease in voltage during the discharge process, thus giving a symmetric charge–discharge cycle. Symmetric charge–discharge curves were observed for Aza-CMPs measured at different current densities (Figure 3b and Figure S15 in the Supporting Information). A general tendency is that when the current density increased, the charge and discharge times were significantly shortened. Aza-CMP@350 can be operated at a high current density of 10 A g^{-1} to allow power supply at high rates (Figure 3b, black curve).

The specific capacitance was evaluated from the discharge curve and found to be highly dependent on the synthesis temperatures of Aza-CMPs (Figure 3c and Table S4 in the Supporting Information). Over the observed current density range from 0.1 to 10 A g^{-1}, Aza-CMP@350, Aza-CMP@400, and Aza-CMP@450 exhibited outstanding capacitance. For example, Aza-CMP@450 had the highest capacitance of 946 F g^{-1} among the members of Aza-CMPs. Other members also exhibited high capacitances of 549–818 F g^{-1}, at a current density of 0.1 A g^{-1}. However, Aza-CMP@500 with small pores could not retain the capacitance especially when the current density was increased up to 5 and 10 A g^{-1}. Similarly, the capacitance of Aza-CMP@300 with low surface area (24 m^2 g^{-1}) showed a significant decrease from 419 to 263 F g^{-1} when the current density was increased from 2 to 5 A g^{-1}. The decrement was more explicit at the current density of 10 A g^{-1} and it displayed a sharp drop to 93 F g^{-1}. The decrement tendencies can be ascribed to the inhibition of ion motion caused by small pores and low surface area.[2d,11a] In contrast, Aza-CMP@350 with a relatively large surface area (546 m^2 g^{-1}) and large pore size (1.4 nm) retains a large capacitance of 397 F g^{-1} at the current density of 5 A g^{-1}. Aza-CMP@350 can be operated at high current density of 10 A g^{-1} to achieve large capacitance of 378 F g^{-1}, which allows rapid charge and power supply.

The specific capacitance of Aza-CMPs was significantly higher, four times than that of activated carbon materials (<270 F g^{-1}).[1,11b] Aza-CMPs are superior to nitrogen-enriched porous carbon materials (50–330 F g^{-1}) and outperform the state-of-the-art nanostructured carbon including template porous carbon (120–350 F g^{-1}),[11c] graphenes (120 F g^{-1}),[1b] carbon nanotubes (50–120 F g^{-1}),[11d] and carbon fibers (120–370 F g^{-1}).[11e] The capacitance is even greater than the best values for supercapacitors (720 F g^{-1}) with a redox-active ruthenium oxide electrode.[11f] The Ragone plot reveals that Aza-CMPs exhibit the maximum energy and power densities of 53 W h kg^{-1} and 2.25 kW kg^{-1}, respectively (see Figure S16 in the Supporting Information). The Ragone plot shows that Aza-CMP@350 is the best among the members of Aza-CMPs at high current density. The energy density is higher than those of nanostructured porous carbon materials and reaches the regime of batteries such as Pb-acid, NiCd, and lithium ion battery (10–150 W h kg^{-1}).[1a] The powder density of Aza-CMPs is more than one order of magnitude higher than those of batteries (< 0.3 kW kg^{-1}).[1a]

The stability of Aza-CMPs was tested by cycling experiments. As demonstrated in Figure 4a, Aza-CMP@350 exhibited excellent performance stability without loss in capaci-

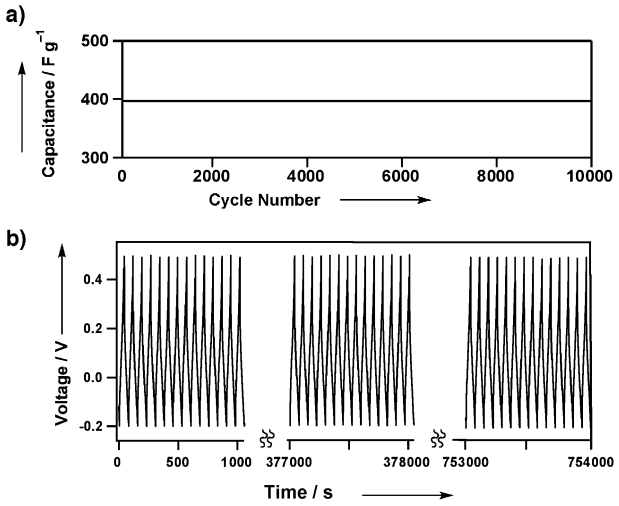

Figure 4. a) Capacitance of Aza-CMP@350 for a 10000-cycle charge–discharge test at a current density of 5 A g^{-1}. b) Charge–discharge curves of Aza-CMP@350 during a test of 10000 cycles. The profiles of three time zones of the initial, middle, and last 1000 seconds are selected to confirm that they are identical to each other in shape and symmetry.

tance (397 F g^{-1}) after 10000 charge–discharge cycles at a current density of 5 A g^{-1}. The charge–discharge profiles retain the linearity and symmetry well (Figure 4b). Aza-CMP@400 also exhibited a highly stable performance without any deterioration (see Figure S17 in the Supporting Information). That is, Aza-CMPs outperform supercapacitors with redox-active electrodes including ruthenium oxide that usually cause a decrease of capacitance after a few cycles. The aza-fused porous framework endow Aza-CMPs with not only large capacitance, high power and energy densities, but an excellent cycle life as well.

To gain insight into the kinetic behavior of Aza-CMPs, electrochemical impedance spectroscopy (EIS) was performed in the frequency range from 10 kHz to 10 mHz. Nyquist plots of Aza-CMPs (Figure 5a) showed intercepts with the Z' axis (real impedance axis) at almost the same position, at around 0.5 Ω. This resistance represents the internal resistance that originates from the resistance of the electrolyte[11a] and has therefore the same value for all of Aza-CMPs. With increment in the Z' value (frequency decrease), Aza-CMPs exhibited semicircle-shaped curves because of the contact resistance between the electrode and current collector.[11a] Aza-CMP@350 had a contact resistance of only 1.4 Ω, which was the lowest interfacial contact resistance among Aza-CMPs (2.2, 2.8, 4.3, and 8.3 Ω for Aza-CMP@400, Aza-CMP@450, Aza-CMP@500, and Aza-CMP@300, respectively).

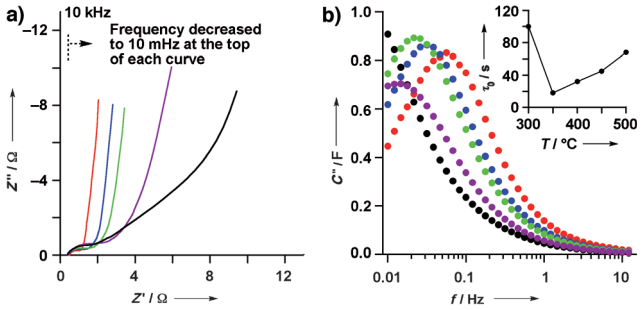

Figure 5. a) Electrochemical impedance spectroscopy (EIS) profiles of Aza-CMPs measured in the frequency range from 10 kHz to 10 mHz (black: Aza-CMP@300; red: Aza-CMP@350; blue: Aza-CMP@400; green: Aza-CMP@450, purple: Aza-CMP@500). b) Plot of imaginary capacitance versus frequency (colors as in (a)). The inset shows a plot of the time constant τ_0 to versus synthesis temperature T.

Aza-CMPs displayed linear plots in the low-frequency region, in which the slope reflects the diffusive resistivity of the electrolyte ions within the pores (Figure 5a). Aza-CMP@350 exhibited a near vertical line that was almost parallel to the Z'' axis (imaginary impedance axis), which indicated ideal capacitive behavior. This was also the case for Aza-CMP@400 and Aza-CMP@450. In contrast, Aza-CMP@500 and Aza-CMP@300 had lines that were significantly inclined from the ideal vertical line, which indicated much higher diffusive resistivity. To evaluate the quantitative frequency response, plots of imaginary capacitance versus frequency were derived from the EIS profiles (Figure 5b). The maximum point of the resultant convex curves represents the frequency f_0, at which purely resistive behavior is transformed into purely capacitive behavior. Aza-CMP@350 exhibited a f_0 value of 0.06 Hz, which became smaller in the order from Aza-CMP@400 > Aza-CMP@450 > Aza-CMP@500 > Aza-CMP@300. The reciprocal of f_0 provides a time constant τ_0 (Figure 5b, inset), which is a quantitative measure of how fast the device can be reversibly charged and discharged. Aza-CMP@350 gave the smallest τ_0 value of 18 s, which increased in the order from Aza-CMP@400 (32 s) < Aza-CMP@450 (46 s) < Aza-CMP@500 (68 s) < Aza-CMP@300 (>100 s). Therefore, Aza-CMP@350 can be charged and discharged in a much shorter time than Aza-CMP@500 and Aza-CMP@300.

These kinetic results provide insight into the supercapacitive energy storage and power supply using Aza-CMPs. The structural factors of Aza-CMPs work co-operatively. First, the skeleton has low interfacial resistance in electric transmission. Second, the dense aza groups increase the density of the electrolyte ions accumulated on the pore walls through electrostatic interactions with protons[8] and facilitate the formation of charge layers. Third, the pore size has a significant effect on the performance of Aza-CMPs. Suitable pore sizes improve the movement of ion species.[11a] This accounts for the deviation from the ideal vertical line of Aza-CMP@500, the pore size (0.85 nm) of which is smaller than the size of the electrolyte ions (sulfuric acid electrolyte (proton): 4.2 Å, sulfate: 5.3 Å). Fourth, a large surface area is necessary to provide an interface for the formation of electrostatic charge-separation layers in the pores. This is related to the low capacitance of the low surface-area Aza-CMP@300. Aza-CMPs that combine the suitable pore size, high surface area, and low interfacial resistance facilitate the charge accumulation and ion motion and as a result endow the framework with outstanding supercapacitive functions.

In summary, we have explored CMPs for supercapacitive energy storage, through the construction of an aza-fused

porous framework with built-in aza units and high surface-area micropores. The fused skeleton, dense aza units, and well-defined micropores work co-operatively and facilitate electrostatic charge-separation layer formation. Consequently, Aza-CMPs exhibit large capacitance, high energy and power densities, and enable repetitive energy storage and power supply with an excellent cycle life. These remarkable results reported herein demonstrate the enormous potential of π-conjugated microporous polymers as high-energy storage devices.

Received: May 21, 2011
Published online: August 12, 2011

Keywords: co-operative phenomena · energy storage · microporous materials · polymers · supercapacitors

[1] a) R. Kötz, M. Carlen, *Electrochim. Acta* **2000**, *45*, 2483 – 2498; b) A. Burke, *J. Power Sources* **2000**, *91*, 37 – 50.
[2] L. L. Zhang, X. S. Zhao, *Chem. Soc. Rev.* **2009**, *38*, 2520 – 2531.
[3] a) A. I. Cooper, *Adv. Mater.* **2009**, *21*, 1291 – 1295; b) A. Thomas, P. Kuhn, J. Weber, M. M. Titirici, M. Antonietti, *Macromol. Rapid Commun.* **2009**, *30*, 221 – 236.
[4] a) J. X. Jiang, F. Su, A. Trewin, C. D. Wood, N. L. Campbell, H. Niu, C. Dickinson, A. Y. Ganin, M. J. Rosseinsky, Y. Z. Khimyak, A. I. Cooper, *Angew. Chem.* **2007**, *119*, 8728 – 8732; *Angew. Chem. Int. Ed.* **2007**, *46*, 8574 – 8578; b) J. X. Jiang, F. Su, A. Trewin, C. D. Wood, H. Niu, J. T. A. Jones, Y. Z. Khimyak, A. I. Cooper, *J. Am. Chem. Soc.* **2008**, *130*, 7710 – 7720; c) J. T. A. Jones, D. Holden, T. Mitra, T. Hasell, D. J. Adams, K. E. Jelfs, A. Trewin, D. J. Willock, G. M. Day, J. Bacsa, A. Steiner, A. I. Cooper, *Angew. Chem.* **2011**, *123*, 775 – 779; *Angew. Chem. Int. Ed.* **2011**, *50*, 749 – 753; d) J. X. Jiang, C. Wang, A. Laybourn, T. Hasell, R. Clowes, Y. Z. Khimyak, J. L. Xiao, S. J. Higgins, D. J. Adams, A. I. Cooper, *Angew. Chem.* **2011**, *123*, 1104 – 1107; *Angew. Chem. Int. Ed.* **2011**, *50*, 1072 – 1075; e) R. Dawson, D. J. Adams, A. I. Cooper, *Chem. Sci.* **2011**, DOI: 10.1039/c1sc00100k.
[5] a) M. J. Bojdys, S. A. Wohlgemuth, A. Thomas, M. Antonietti, *Macromolecules* **2010**, *43*, 6639 – 6645; b) X. C. Wang, K. Maeda, A. Thomas, K. Takanabe, G. Xin, J. M. Carlsson, K. Domen, M. Antonietti, *Nat. Mater.* **2009**, *8*, 76 – 80; c) R. Palkovits, M. Antonietti, P. Kuhn, A. Thomas, F. Schüth, *Angew. Chem.* **2009**, *121*, 7042 – 7045; *Angew. Chem. Int. Ed.* **2009**, *48*, 6909 – 6912; d) A. Thomas, *Angew. Chem.* **2010**, *122*, 8506 – 8523; *Angew. Chem. Int. Ed.* **2010**, *49*, 8328 – 8344.
[6] a) L. Chen, Y. Yang, D. Jiang, *J. Am. Chem. Soc.* **2010**, *132*, 9138 – 9143; b) L. Chen, Y. Honsho, S. Seki, D. Jiang, *J. Am. Chem. Soc.* **2010**, *132*, 6742 – 6748; c) L. Chen, Y. Yang, Z. Guo, D. Jiang, *Adv. Mater.* **2011**, DOI: 10.1002/adma.201100974.
[7] X. Zhang, C. Wang, K. E. deKrafft, W. Lin, *J. Am. Chem. Soc.* **2011**, *133*, 2056 – 2059.
[8] a) A. Albert, R. Goldacre, J. Phillips, *J. Chem. Soc.* **1948**, 2240 – 2249; b) K. Gotoh, T. Asaji, H. Ishida, *Acta Crystallogr. Sect. C* **2007**, *63*, o17 – o20.
[9] L. Sabbatini, C. Malitesta, E. De Giglio, I. Losito, L. Torsi, P. G. Zambonin, *J. Electron Spectrosc. Relat. Phenom.* **1999**, *100*, 35 – 53.
[10] A. Saito, H. C. Foley, *AIChE J.* **1991**, *37*, 429 – 436.
[11] a) C. Largeot, C. Portet, J. Chmiola, P. Taberna, Y. Gogotsi, P. Simon, *J. Am. Chem. Soc.* **2008**, *130*, 2730 – 2731; b) E. Raymundo-Piñero, M. Cadek, F. Béguin, *Adv. Funct. Mater.* **2009**, *19*, 1032 – 1039; c) H. Yamada, H. Nakamura, F. Nakahara, I. Moriguchi, T. Kudo, *J. Phys. Chem. C* **2007**, *111*, 227 – 233; d) X. L. Feng, Y. Y. Liang, L. J. Zhi, A. Thomas, D. Q. Wu, I. Lieberwirth, U. Kolb, K. Müllen, *Adv. Funct. Mater.* **2009**, *19*, 2125 – 2129; e) B. Xu, F. Wu, R. J. Chen, G. P. Cao, S. Chen, Z. M. Zhou, Y. S. Yang, *Electrochem. Commun.* **2008**, *10*, 795 – 797; f) J. P. Zheng, P. J. Cygan, T. R. Jow, *J. Electrochem. Soc.* **1995**, *142*, 2699 – 2703.

